

1

Fundamentals of Optics

Ting-Chung Poon and Jung-Ping Liu

1.1

Introduction

In this chapter, we discuss some of the fundamentals of optics. We first cover the electromagnetic (EM) spectrum, which shows that the visible spectrum occupies just a very narrow portion of the entire EM spectrum. We then discuss geometrical optics and wave optics. In geometrical optics, we formulate the propagation of light rays in terms of matrices, whereas in wave optics we formulate wave propagation using the Fresnel diffraction formula, which is the solution to Maxwell's equations. Fourier optics and its applications in optical image processing are then discussed. One of the important optical image processing applications in optical correlation is subsequently explained. Finally, we discuss the human visual system and end this chapter with a brief conclusion.

1.2

The Electromagnetic Spectrum

James Clerk Maxwell (1831–1879) used his famous Maxwell's equations to show that EM waves exhibit properties similar to those of visible light. After continuous studies of optical and EM waves in the last century, we have finally understood that visible light is only a narrow band in the EM spectrum. Figure 1.1 shows the complete EM spectrum. It consists of regions of radio waves, microwaves, infrared (IR), visible light, ultraviolet (UV), X-rays, and γ -rays.

Visible light is the EM radiation that can be observed by human eyes directly. Because of the various receptors in human eyes (see Section 1.7), people can identify EM radiation of different wavelengths by their colors. Visible light can be roughly separated into violet (390–455 nm), blue (455–492 nm), green (492–577 nm), yellow (577–597 nm), orange (597–622 nm), and red (622–780 nm). Beyond the red end of the visible band lies the IR region. It contains the near infrared (NIR, 0.78–3 μm), the middle infrared (MIR, 3.0–6.0 μm), the far infrared (FIR, 6.0–15 μm), and the extreme infrared (XIR, 15–1000 μm). There are also other nomenclatures

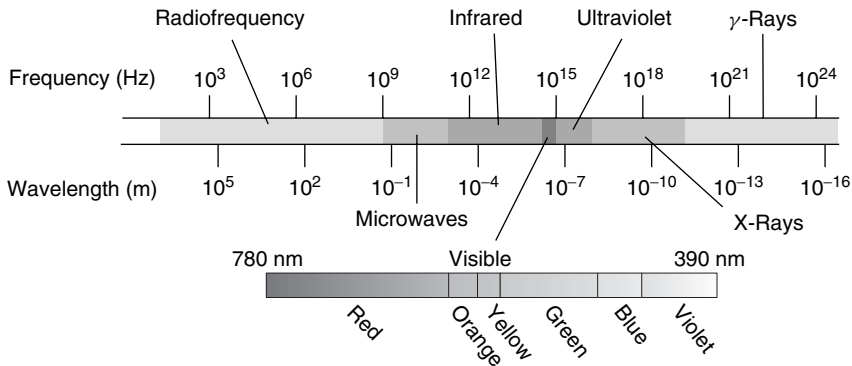


Figure 1.1 The electromagnetic spectrum.

and division schemes, depending on the purposes of the applications and the users [1]. The IR imaging technique is applied in astronomical measurements, thermographs, heat targets, and noninvasive medical imaging of subcutaneous tissues. The band merging into the violet end of the visible light is the UV region. Its spectrum range is roughly between 1.0 and 390 nm. UV radiation is used as the light source for lithography to achieve narrower linewidth. Sometimes, the visible band, together with parts of the UV and IR regions, is classified as the *optical region*, in which we use similar ways to produce, to modulate, and to measure the optical radiation.

At the long-wavelength end of the EM spectrum are microwaves and radio waves. Their ranges are from 3×10^{11} to 10^9 Hz, and from 10^9 Hz to very low frequency, respectively. The radiations in this region exhibit more wave properties, and are usually applied to remote sensing and communications. Although antennae are used to produce and to receive microwaves and radio waves, we can still perform imaging in this region, especially for astronomical measurements [2]. It is worth noting that the spectrum range between FIR and microwaves, namely, from 0.1 to 10 THz, is called the *terahertz band (THz band)*. The THz band covers the millimeter wave (MMW, 0.03–0.3 THz), the submillimeter wave (SMMW, 0.3–3 THz), and the FIR regions. Terahertz radiation is highly absorbed by water and reflected by metals. Thus terahertz imaging has unique applications in nondestructive testing, biomedical imaging, and remote sensing.

At the short-wavelength end of the EM spectrum are the X-rays and γ -rays. X-rays, ranging from 1.0 nm to 6.0 pm, can pass through the soft tissues easily and are thus widely used in applications in medical imaging. The X-ray lasers and their related imaging techniques have been studied for decades and are still under development [3]. Since the wavelength of X-rays is shorter than UV rays, the success of X-ray imaging techniques will lead to a greater improvement of image resolution. γ -Rays have the shortest wavelength and thus they possess very high photon energy ($> 10^4$ eV) and behave more like particles. γ -Rays have been applied in medical imaging because of their excellent depth of penetration into soft tissues and their high resolution. For example, Technetium-99m or ^{99m}Tc is the most commonly used γ -ray-emitting radionuclide in radiopharmacology,

and it produces γ -radiation with principal photon energy of 140 keV. Another nuclear medicine technique called *positron emission tomography (PET)* is also an imaging technique of 511 keV γ -radiation resulting from the annihilation of positron–electron pairs of a radionuclide.

1.3 Geometrical Optics

In *geometrical optics*, light is treated as particles called *photons* and the trajectories that these photons follow are termed *rays*. Hence geometrical optics is also known as *ray optics*. Ray optics is based on *Fermat's principle*, which states that the path that a light ray follows is an extremum in comparison to nearby paths. Usually the extremum is a minimum. As a simple example shown in Figure 1.2, the shortest distance, that is, the minimum distance, between two points A and B is along a straight line (solid line) in a *homogeneous medium* (medium with a constant refractive index). Hence the light ray takes the solid line as a path instead of taking the nearby dotted line. By the same token, according to Fermat's principle, we can derive the laws of reflection and refraction [4]. The law of refraction, which describes a light ray entering from one medium, characterized by refractive index n_i , into another medium of refractive index n_t , is given by

$$n_i \sin \theta_i = n_t \sin \theta_t \quad (1.1)$$

where θ_i and θ_t are the angles of incidence and transmission (or refraction), respectively, as shown in Figure 1.3. The angles are measured from the normal NN' to the interface MM', which separates the two media.

1.3.1 Ray Transfer Matrix

To describe ray propagation through optical systems comprising, for instance, a succession of lenses all centered on the same axis called the *optical axis*, we can use matrix formalism if we consider *paraxial rays*. Figure 1.4 depicts the system coordinates and parameters under consideration. We take the optical axis along

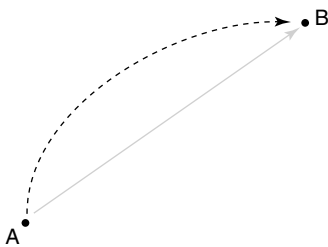


Figure 1.2 A light ray takes the shortest distance, a straight line (solid line), between two points in a homogeneous medium.

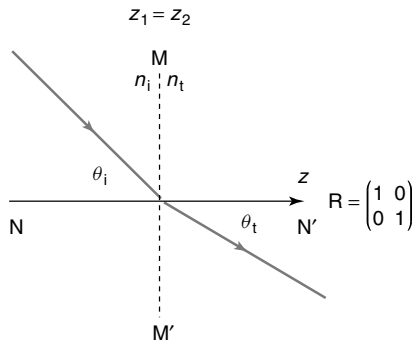


Figure 1.3 Law of refraction and its transfer matrix R .

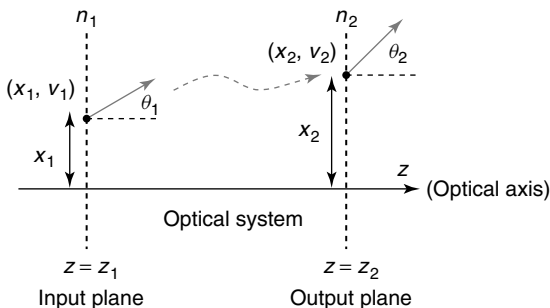


Figure 1.4 Input and output planes in an optical system.

the z -axis, which is the general direction in which the rays travel. Paraxial rays lie only in the x - z plane and are close to the z -axis. In other words, paraxial rays are rays with angles of incidence, reflection, and refraction at an interface, satisfying the small-angle approximation in that $\tan \theta \approx \sin \theta \approx \theta$ and $\cos \theta \approx 1$, where the angle θ is measured in radians. *Paraxial optics* deals with paraxial rays. Hence in paraxial optics, the law of refraction simplifies to

$$n_i \theta_i = n_t \theta_t \tag{1.2}$$

A ray at a given x - z plane may be specified by its *height* x from the optical axis and by its angle θ or *slope* that it makes with the z -axis. The convention for the angle is anticlockwise positive measured from the z -axis. The height x of a point on a ray is taken positive if the point lies above the z -axis and negative if it is below the z -axis. The quantities (x, θ) , therefore, represent the coordinates of the ray for a given z -plane. It is customary to replace the corresponding angle θ by $v = n\theta$, where n is the refractive index at the z -constant plane. Therefore, as shown in Figure 1.4, the ray at $z = z_1$ passes through the input plane with input ray coordinates $(x_1, n_1\theta_1)$ or (x_1, v_1) . If the output ray coordinates at $z = z_2$, the output plane, are $(x_2, n_2\theta_2)$ or (x_2, v_2) , we can relate the input coordinates to the output coordinates by a 2×2

matrix as follows:

$$\begin{pmatrix} x_2 \\ v_2 \end{pmatrix} = \begin{pmatrix} A & B \\ C & D \end{pmatrix} \begin{pmatrix} x_1 \\ v_1 \end{pmatrix} \quad (1.3)$$

The above $ABCD$ matrix is called the *ray transfer matrix*, which can be made up of many matrices to account for the effects of the ray passing through various optical elements such as lenses. Equation (1.3) is equivalently given by

$$x_2 = Ax_1 + Bv_1 \quad (1.4a)$$

$$v_2 = Cx_1 + Dv_1 \quad (1.4b)$$

Hence, the law of refraction given by Eq. (1.2) can be written as

$$\begin{pmatrix} x_2 \\ v_2 \end{pmatrix} = \begin{pmatrix} 1 & 0 \\ 0 & 1 \end{pmatrix} \begin{pmatrix} x_1 \\ v_1 \end{pmatrix} = \mathbf{R} \begin{pmatrix} x_1 \\ v_1 \end{pmatrix} \quad (1.5)$$

where $v_2 = n_2\theta_t = n_t\theta_t$ and $v_1 = n_1\theta_i = n_t\theta_i$. Therefore, the $ABCD$ matrix for the law of refraction is $\mathbf{R} = \begin{pmatrix} 1 & 0 \\ 0 & 1 \end{pmatrix}$ and Figure 1.3 summarizes the matrix formalism for the law of refraction. From Eq. (1.5), we see that $x_2 = x_1$ as the heights of the input and output rays are the same. Also, $v_2 = v_1$, which gives the law of refraction, $n_t\theta_t = n_i\theta_i$. We also notice that the input and output planes in this case are the same plane at $z = z_1 = z_2$.

Figure 1.5 shows two more useful ray transfer matrices: the *translation matrix* \mathbf{T} and the *thin-lens matrix* \mathbf{L} . The translation matrix describes the ray undergoing a translation of distance d in a homogeneous medium characterized by n and the

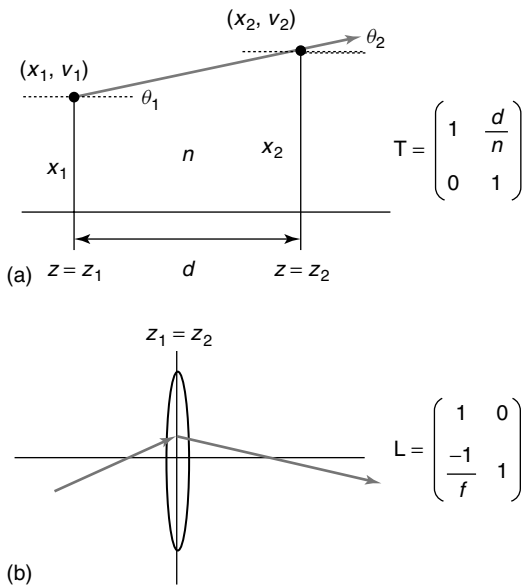


Figure 1.5 (a) Translation matrix and (b) lens matrix.

matrix equation is given as follows:

$$\begin{pmatrix} x_2 \\ v_2 \end{pmatrix} = \begin{pmatrix} 1 & \frac{d}{n} \\ 0 & 1 \end{pmatrix} \begin{pmatrix} x_1 \\ v_1 \end{pmatrix} = \mathbf{T} \begin{pmatrix} x_1 \\ v_1 \end{pmatrix} \quad (1.6a)$$

where $v_2 = n\theta_2$, $v_1 = n\theta_1$, and

$$\mathbf{T} = \begin{pmatrix} 1 & \frac{d}{n} \\ 0 & 1 \end{pmatrix} \quad (1.6b)$$

Note that when the ray is undergoing translation as shown in Figure 1.5a in a homogeneous medium, $\theta_1 = \theta_2$ and therefore $v_1 = v_2$ as given by Eq. (1.6a). From Eq. (1.6a), we also see that $x_2 = x_1 + dv_1/n = x_1 + d\theta_1$. Hence x_2 is $d\theta_1$ higher than x_1 , consistent with the situation shown in Figure 1.5a. When a thin converging lens of focal length f is involved, the matrix equation is

$$\begin{pmatrix} x_2 \\ v_2 \end{pmatrix} = \begin{pmatrix} 1 & 0 \\ -\frac{1}{f} & 1 \end{pmatrix} \begin{pmatrix} x_1 \\ v_1 \end{pmatrix} = \mathbf{L} \begin{pmatrix} x_1 \\ v_1 \end{pmatrix} \quad (1.7a)$$

where \mathbf{L} is the *thin-lens matrix* given by

$$\mathbf{L} = \begin{pmatrix} 1 & 0 \\ -\frac{1}{f} & 1 \end{pmatrix} \quad (1.7b)$$

By definition, a lens is thin when its thickness is assumed to be zero and hence the input plane and the output plane have become the same plane or $z_1 = z_2$ as shown in Figure 1.5b. We also have $x_1 = x_2$ as the heights of the input and output rays are the same for the thin lens. Regarding the slope, from Eq. (1.7a), we have $v_2 = -\frac{1}{f}x_1 + v_1$. For $v_1 = 0$, that is, the input ray is parallel to the optical axis, $v_2 = -\frac{1}{f}x_1 = -\frac{1}{f}x_2$. For positive x_1 , $v_2 < 0$, since $f > 0$ for a converging lens. For negative x_1 , $v_2 > 0$. Hence all input rays parallel to the optical axis converge behind the lens to a point called the *back focal point*, that is, at a distance f away from the lens. Note that for a thin lens, the front focal point is also a distance f away from but in front of the lens. For the input ray coordinates given by $(x_1, x_1/f)$ and according to Eq. (1.7), the output ray coordinates are $(x_2 = x_1, 0)$, which implies that all output rays will be parallel to the optical axis as $v_2 = 0$. This is the case that all rays passing through the front focal point of a lens will give rise to parallel output rays. The output plane that contains the back focal point is called the *back focal plane* and, similarly, the plane that contains the front focal point is the *front focal plane*.

1.3.2

Two-Lens Imaging System

Figure 1.6 shows a more complicated optical system as an example. The system is a two-lens imaging system with lenses L_1 and L_2 of focal lengths f_1 and f_2 , respectively, and the two lenses are separated by a distance $f_1 + f_2$. The object is placed in the front focal plane of lens L_1 . We can relate the input ray coordinates (x_1, v_1) and the output ray coordinates (x_2, v_2) using the ray transfer matrices.

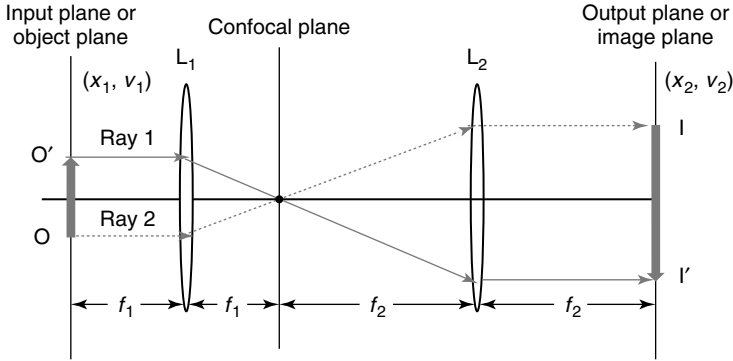


Figure 1.6 Two-lens imaging system.

Therefore, from Eq. (1.6), we first relate the input coordinates (x_1, v_1) on the input plane to the ray coordinates (x'_1, v'_1) , located on a plane immediately before the lens L_1 by

$$\begin{pmatrix} x'_1 \\ v'_1 \end{pmatrix} = \begin{pmatrix} 1 & f_1 \\ 0 & 1 \end{pmatrix} \begin{pmatrix} x_1 \\ v_1 \end{pmatrix} \quad (1.8)$$

where we have assumed that the two-lens system is immersed in air, that is, $n = 1$. The distance of ray transfer is $d = f_1$. Now we relate (x'_1, v'_1) to (x''_1, v''_1) , the ray coordinates located on a plane immediately after the lens L_1 by

$$\begin{pmatrix} x''_1 \\ v''_1 \end{pmatrix} = \begin{pmatrix} 1 & 0 \\ \frac{-1}{f_1} & 1 \end{pmatrix} \begin{pmatrix} x'_1 \\ v'_1 \end{pmatrix} \quad (1.9)$$

where we have used the lens matrix in Eq. (1.7) with $f = f_1$. Now by substituting Eq. (1.9) into Eq. (1.8), we can relate the input ray coordinates (x_1, v_1) to the ray coordinates (x''_1, v''_1) just after the lens L_1 :

$$\begin{pmatrix} x''_1 \\ v''_1 \end{pmatrix} = \begin{pmatrix} 1 & 0 \\ \frac{-1}{f_1} & 1 \end{pmatrix} \begin{pmatrix} 1 & f_1 \\ 0 & 1 \end{pmatrix} \begin{pmatrix} x_1 \\ v_1 \end{pmatrix} \quad (1.10)$$

Note that the overall system matrix so far is expressed in terms of the product of two matrices written in order from right to left as the ray transverses from left to right on the optical axis. By the same token, we can show that the input ray coordinates (x_1, v_1) and the final output ray coordinates (x_2, v_2) on the image plane are connected using five ray transfer matrices (three translation matrices and two-lens matrices):

$$\begin{pmatrix} x_2 \\ v_2 \end{pmatrix} = \mathbf{S} \begin{pmatrix} x_1 \\ v_1 \end{pmatrix} \quad (1.11a)$$

where \mathbf{S} is *system matrix* of the overall system and is given by

$$\mathbf{S} = \begin{pmatrix} 1 & f_2 \\ 0 & 1 \end{pmatrix} \begin{pmatrix} 1 & 0 \\ \frac{-1}{f_2} & 1 \end{pmatrix} \begin{pmatrix} 1 & f_1 + f_2 \\ 0 & 1 \end{pmatrix} \begin{pmatrix} 1 & 0 \\ \frac{-1}{f_1} & 1 \end{pmatrix} \begin{pmatrix} 1 & f_1 \\ 0 & 1 \end{pmatrix} \quad (1.11b)$$

The system matrix \mathbf{S} can be simplified to

$$\mathbf{S} = \begin{pmatrix} -\frac{f_2}{f_1} & 0 \\ 0 & -\frac{f_1}{f_2} \end{pmatrix} \quad (1.12)$$

and Eq. (1.11a) becomes

$$\begin{pmatrix} x_2 \\ v_2 \end{pmatrix} = \begin{pmatrix} -\frac{f_2}{f_1} & 0 \\ 0 & -\frac{f_1}{f_2} \end{pmatrix} \begin{pmatrix} x_1 \\ v_1 \end{pmatrix} \quad (1.13)$$

From the above equation, we can find, for example, $x_2 = -\frac{f_2}{f_1}x_1$; and the lateral magnification M of the imaging system is found to be

$$M = \frac{x_2}{x_1} = -\frac{f_2}{f_1} \quad (1.14)$$

Since both the focal lengths of the converging lenses are positive, $M < 0$ signifies that the image formed is real and inverted as shown in Figure 1.6. In addition, if $f_2 > f_1$, as is the case illustrated in Figure 1.6, we have a magnified image. In the figure, we show a ray diagram, illustrating an image formation of the system. A ray (Ray 1 in the Figure 1.6) coming from O' parallel to the optical axis hits the image point I' and a ray (Ray 2) from the object point O parallel to the optical axis hits the image point I .

1.3.3

Aberrations

In the preceding section, we have introduced the basic concepts of an imaging system in which a point object will produce a point image using paraxial rays. In real optical systems, nonparaxial rays are also involved in image formation and the actual image departs from the ideal point image. In fact, these rays form a blur spot instead of a single point image. This departure from ideal image formation is known as *aberrations*.

Aberrations are usually due to the deviation from the paraxial approximation, but this is not always so. We also have defocus aberration and chromatic aberration because these aberrations also result in a blurred image spot. However, the former is due to the mismatch between the observation plane and the image plane, while the latter is due to the various refractive indices of the same material at different wavelengths.

To systematically analyze the aberrations, we can expand the sine of the angle between the ray and the optical axis, that is, $\sin \theta \approx \theta - \theta^3/3! + \theta^5/5! - \dots$. The first expansion term is also what we use in the paraxial approximation (Eq. (1.2)), which leads to an ideal image point due to an ideal object point. Aberrations that come about from neglecting the second term in the expansion are called *third-order aberrations*, while the fifth-order aberrations arise from neglecting the third term in the expansion. Usually, in aberration analysis we only need to consider the third-order aberrations. The effect of fifth-order and higher order aberrations are

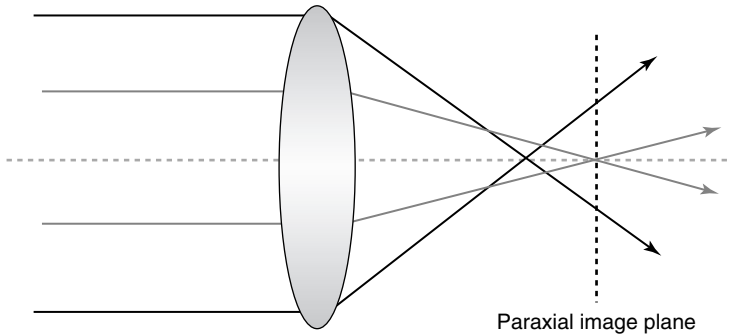


Figure 1.7 Spherical aberration on a single lens.

complicated and minor, and these are only considered in high-precision optical systems. Spherical aberration is one of the five third-order aberrations, and it is easily found in a low-cost single lens. We can consider the imaging of a general spherical lens, in which a point object is set at infinity as shown in Figure 1.7. The light rays near the center of the lens are converged to the paraxial image plane (back focal plane). The light rays passing through the periphery of the lens also converge, but the image point deviates from the paraxial image point. As a result, the image of a point in the image plane is not an infinitesimal point but a blurred spot. Spherical aberration is a function of the lens profile, the lens thickness, the lens diameter, and the object distance (or equivalently, the image distance). The easiest way to reduce spherical aberration is to shorten the effective diameter of the lens. However, the light intensity is reduced accordingly. Alternatively, spherical aberration can be minimized by using an aspheric surface (departing from spherical) on a single lens or by using several lenses.

Besides spherical aberration, there are also coma, astigmatism, field curvature, and distortion that comprise the third-order aberrations. The readers may consult Chapters 13 and 25 of this book or other books for more details [2, 5–7]. Finally, it may be noted that even if the optical system is free from all the third- and high-order aberrations, we still cannot accomplish an infinitesimal image point because of diffraction effects (see Section 1.5).

1.4

Maxwell's Equations and the Wave Equation

In geometrical optics, we treat light as particles. In *wave optics*, we treat light as waves. Wave optics accounts for wave effects such as interference and diffraction. Maxwell's equations form the starting point for wave optics:

$$\nabla \cdot \mathbf{D} = \rho_v \quad (1.15)$$

$$\nabla \cdot \mathbf{B} = 0 \quad (1.16)$$

$$\nabla \times \mathbf{E} = -\frac{\partial \mathbf{B}}{\partial t} \quad (1.17)$$

$$\nabla \times \mathbf{H} = \mathbf{J} = \mathbf{J}_C + \frac{\partial \mathbf{D}}{\partial t} \quad (1.18)$$

where, in these equations, we have four vector quantities called *electromagnetic fields*: the electric field strength \mathbf{E} (V m^{-1}), the electric flux density \mathbf{D} (C m^{-2}), the magnetic field strength \mathbf{H} (A m^{-1}), and the magnetic flux density \mathbf{B} (Wb m^{-2}). The vector quantity \mathbf{J}_C and the scalar quantity ρ_v are the current density (A m^{-2}) and the electric charge density (C m^{-3}), respectively, and they are the sources responsible for generating the EM fields. In addition to Maxwell's equations, we have the constitutive relations:

$$\mathbf{D} = \varepsilon \mathbf{E} \quad (1.19)$$

and

$$\mathbf{B} = \mu \mathbf{H} \quad (1.20)$$

where ε and μ are the permittivity (F m^{-1}) and permeability (H m^{-1}) of the medium, respectively. In this chapter, we take ε and μ to be scalar constants, which is the case for a linear, homogeneous, and isotropic medium such as in vacuum. Using Eqs (1.15–1.20), we can derive a wave equation in \mathbf{E} or \mathbf{B} [8]. For example, the wave equation in \mathbf{E} is

$$\nabla^2 \mathbf{E} - \mu \varepsilon \frac{\partial^2 \mathbf{E}}{\partial t^2} = \mu \frac{\partial \mathbf{J}_C}{\partial t} + \frac{1}{\varepsilon} \nabla \rho_v \quad (1.21)$$

where $\nabla^2 = \frac{\partial^2}{\partial x^2} + \frac{\partial^2}{\partial y^2} + \frac{\partial^2}{\partial z^2}$ is the Laplacian operator in Cartesian coordinates. For a source-free medium, that is, $\mathbf{J}_C = 0$ and $\rho_v = 0$, Eq. (1.21) reduces to the homogeneous wave equation:

$$\nabla^2 \mathbf{E} - \mu \varepsilon \frac{\partial^2 \mathbf{E}}{\partial t^2} = 0 \quad (1.22)$$

Note that $v = 1/\sqrt{\mu\varepsilon}$ is the velocity of the wave in the medium. Equation (1.22) is equivalent to three scalar equations, one for every component of \mathbf{E} . Let

$$\mathbf{E} = E_x \mathbf{a}_x + E_y \mathbf{a}_y + E_z \mathbf{a}_z \quad (1.23)$$

where \mathbf{a}_x , \mathbf{a}_y , and \mathbf{a}_z are the unit vectors in the x , y , and z directions, respectively. Equation (1.22) then becomes

$$\left(\frac{\partial^2}{\partial x^2} + \frac{\partial^2}{\partial y^2} + \frac{\partial^2}{\partial z^2} \right) (E_x \mathbf{a}_x + E_y \mathbf{a}_y + E_z \mathbf{a}_z) = \mu \varepsilon \frac{\partial^2}{\partial t^2} (E_x \mathbf{a}_x + E_y \mathbf{a}_y + E_z \mathbf{a}_z) \quad (1.24)$$

Comparing the \mathbf{a}_x -component on both sides of the above equation gives us

$$\frac{\partial^2 E_x}{\partial x^2} + \frac{\partial^2 E_x}{\partial y^2} + \frac{\partial^2 E_x}{\partial z^2} = \mu \varepsilon \frac{\partial^2 E_x}{\partial t^2}$$

Similarly, we have the same type of equation shown above for the E_y and E_z components by comparing other components in Eq. (1.24). Hence we can write a

compact equation for the three components as follows:

$$\frac{\partial^2 \psi}{\partial x^2} + \frac{\partial^2 \psi}{\partial y^2} + \frac{\partial^2 \psi}{\partial z^2} = \mu \varepsilon \frac{\partial^2 \psi}{\partial t^2} \quad (1.25a)$$

or

$$\nabla^2 \psi = \mu \varepsilon \frac{\partial^2 \psi}{\partial t^2} \quad (1.25b)$$

where ψ may represent a component, E_x , E_y , or E_z , of the electric field \mathbf{E} . Equation (1.25) is called the *scalar wave equation*.

1.5 Wave Optics and Diffraction

In the study of wave optics, we start from the scalar wave equation. Let us look at some of the simplest solutions. One of the simplest solutions is the plane wave solution:

$$\psi(x, y, z, t) = A \exp[i(\omega_0 t - \mathbf{k}_0 \cdot \mathbf{R})] \quad (1.26)$$

where ω_0 is the oscillating angular frequency (rad s^{-1}), $\mathbf{k}_0 = k_{0x} \mathbf{a}_x + k_{0y} \mathbf{a}_y + k_{0z} \mathbf{a}_z$ is the propagation vector, and $\mathbf{R} = x \mathbf{a}_x + y \mathbf{a}_y + z \mathbf{a}_z$ is the position vector. The magnitude of \mathbf{k}_0 is called *wavenumber* and is $|\mathbf{k}_0| = k_0 = \sqrt{k_{0x}^2 + k_{0y}^2 + k_{0z}^2} = \omega_0/v$ with v being the velocity of the wave in the medium given by $v = 1/\sqrt{\mu \varepsilon}$. If the medium is free space, $v = c$ (the speed of light in vacuum) and $|\mathbf{k}_0|$ becomes the wavenumber in free space. Equation (1.26) is a plane wave of amplitude A , traveling along the \mathbf{k}_0 direction. If a plane wave is propagating along the positive z -direction, Eq. (1.26) becomes

$$\psi(z, t) = A \exp[i(\omega_0 t - k_0 z)] \quad (1.27)$$

Equation (1.27) is a complex representation of a plane wave and since the EM fields are real functions of space and time, we can represent the plane wave in real terms by taking the real part of ψ to get

$$\text{Re}\{\psi(z, t)\} = A \cos(\omega_0 t - k_0 z) \quad (1.28)$$

For a plane wave incident on an aperture or a diffracting screen, that is, an opaque screen with some openings allowing light to pass through, the field distribution exiting the aperture or the diffracted field is a little more complicated to find. To tackle the diffraction problem, we need to find the solution of the scalar wave equation under some initial condition. Let us assume the aperture is represented by a transparency function, $t(x, y)$, located on the plane $z = 0$ as shown in Figure 1.8. A plane wave of amplitude A is incident on it. Hence at $z = 0$, according to Eq. (1.27), the plane wave immediately in front of the aperture is given by $A \exp(i\omega_0 t)$. The field immediately after the aperture is

$$\begin{aligned} \psi(x, y, z = 0, t) &= A t(x, y) \exp(i\omega_0 t) = \psi_p(x, y; z = 0) \exp(i\omega_0 t) \\ &= \psi_{p0}(x, y) \exp(i\omega_0 t) \end{aligned} \quad (1.29)$$

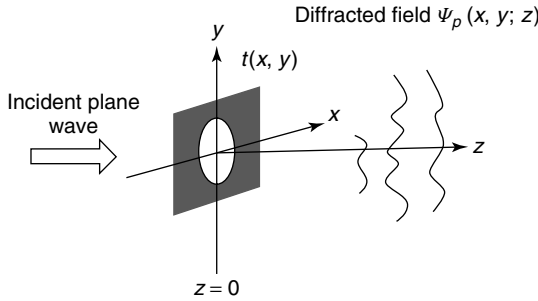


Figure 1.8 Diffraction geometry: $t(x, y)$ is the diffracting screen.

where we have assumed that the aperture is infinitively thin. $\psi_p(x, y; z = 0)$ or $\psi_{p0}(x, y)$ is called the *initial condition*. In the present case, the initial condition of the complex wave is given by $\psi_{p0}(x, y) = A \times t(x, y)$, the amplitude of the incident plane wave multiplied by the transparency function of the aperture. To find the field distribution at a distance z away from the aperture, we model the solution in the form of

$$\psi(x, y, z, t) = \psi_p(x, y; z) \exp(i\omega_0 t) \quad (1.30)$$

where $\psi_p(x, y; z)$ is the unknown to be found. In optics, $\psi_p(x, y; z)$ is called a *complex amplitude*. In engineering, it is known as a *phasor*. To find $\psi_p(x, y; z)$, we substitute Eq. (1.30) into Eq. (1.25). With the given initial condition $\psi_{p0}(x, y)$, we find [8]

$$\begin{aligned} \psi_p(x, y; z) = \exp(-ik_0 z) \frac{ik_0}{2\pi z} \int_{-\infty}^{\infty} \int_{-\infty}^{\infty} \psi_{p0}(x', y') \\ \times \exp\left\{ \frac{-ik_0}{2z} [(x - x')^2 + (y - y')^2] \right\} dx' dy' \end{aligned} \quad (1.31)$$

Equation (1.31) is called the *Fresnel diffraction formula* and describes the Fresnel diffraction of a “beam” during propagation and having an initial complex amplitude given by $\psi_{p0}(x, y)$. The Fresnel diffraction formula has been derived under the following conditions: (i) z must be many wavelengths away from the aperture and (ii) it should be valid under the paraxial approximation, that is, $z^2 \gg x^2 + y^2$. The Fresnel diffraction formula can be written in a compact form if we make use of the convolution integral

$$g(x, y) = g_1(x, y) * g_2(x, y) = \int_{-\infty}^{\infty} \int_{-\infty}^{\infty} g_1(x', y') g_2(x - x', y - y') dx' dy' \quad (1.32)$$

where $*$ denotes convolution of two functions $g_1(x, y)$ and $g_2(x, y)$. We also define a function

$$h(x, y; z) = \exp(-ik_0 z) \frac{ik_0}{2\pi z} \exp\left[\frac{-ik_0}{2z} (x^2 + y^2) \right] \quad (1.33)$$

With Eqs (1.32) and (1.33), the Fresnel diffraction formula can be written simply as

$$\psi_p(x, y; z) = \psi_{p0}(x, y) * h(x, y; z) \quad (1.34)$$

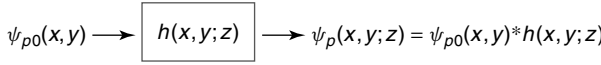


Figure 1.9 Block diagram summarizing Fresnel diffraction.

Hence Fresnel diffraction can be considered as a linear and space-invariant system [8] with input given by $\psi_{p0}(x, y)$ and with the system's impulse response given by $h(x, y; z)$. In optics, $h(x, y; z)$ is called *free-space spatial impulse response*. Figure 1.9 is a block diagram, which summarizes the Fresnel diffraction of a beam with initial profile $\psi_{p0}(x, y)$.

If we have a situation such that the calculation of the diffraction pattern is at distances far away from the aperture, Eq. (1.31) can be simplified. To see how this can be done, let us complete the square in the exponential function and then rewrite Eq. (1.31) to become

$$\begin{aligned} \psi_p(x, y; z) = & \exp(-ik_0z) \frac{ik_0}{2\pi z} \exp\left[\frac{-ik_0}{2z}(x^2 + y^2)\right] \int_{-\infty}^{\infty} \int_{-\infty}^{\infty} \psi_{p0}(x', y') \\ & \times \exp\left\{\frac{-ik_0}{2z}[(x')^2 + (y')^2]\right\} \exp\left[\frac{ik_0}{z}(xx' + yy')\right] dx' dy' \end{aligned} \quad (1.35)$$

In the above integral, ψ_{p0} is considered as the “source,” and therefore the coordinates x' and y' can be called the *source plane*. In order to find the field distribution ψ_p on the observation plane, or the x - y plane, we need to have the source multiplied by the two exponential functions as shown inside the integrand of Eq. (1.35), and then to integrate over the source coordinates. The result of the integration is then multiplied by the factor $\exp(-ik_0z) \frac{ik_0}{2\pi z} \exp\left[\frac{-ik_0}{2z}(x^2 + y^2)\right]$ to arrive at the final result on the observation plane given by Eq. (1.35). Note that the integral in Eq. (1.35) can be simplified if the approximation below is true:

$$\frac{k_0}{2}[(x')^2 + (y')^2]_{\max} = \frac{\pi}{\lambda_0}[(x')^2 + (y')^2]_{\max} \ll z \quad (1.36)$$

The term $\pi[(x')^2 + (y')^2]_{\max}$ is like the maximum area of the source and if this area divided by the wavelength is much less than the distance z under consideration, the term $\exp\left\{\frac{-ik_0}{2z}[(x')^2 + (y')^2]\right\}$ inside the integrand can be considered to be unity, and hence Eq. (1.35) becomes

$$\begin{aligned} \psi_p(x, y; z) = & \exp(-ik_0z) \frac{ik_0}{2\pi z} \exp\left[\frac{-ik_0}{2z}(x^2 + y^2)\right] \int_{-\infty}^{\infty} \int_{-\infty}^{\infty} \psi_{p0}(x', y') \\ & \times \exp\left[\frac{ik_0}{z}(xx' + yy')\right] dx' dy' \end{aligned} \quad (1.37)$$

Equation (1.37) is the *Fraunhofer diffraction formula* and is the limiting case of Fresnel diffraction. Equation (1.36) is therefore called the *Fraunhofer approximation* or the *far field approximation* as diffraction is observed beyond the distance of near-field (Fresnel) diffraction.

1.6 Fourier Optics and Applications

Fourier optics is a term used by many authors to describe the use of Fourier transform to analyze problems in wave optics [8]. We first introduce the definition of Fourier transform and then we formulate wave optics using the transform. The two-dimensional spatial Fourier transform of a signal $f(x, y)$ is given by

$$\mathcal{F}\{f(x, y)\} = F(k_x, k_y) = \int_{-\infty}^{\infty} \int_{-\infty}^{\infty} f(x, y) \exp(ik_x x + ik_y y) dx dy \quad (1.38)$$

and its inverse Fourier transform is

$$\mathcal{F}^{-1}\{F(k_x, k_y)\} = f(x, y) = \frac{1}{4\pi^2} \int_{-\infty}^{\infty} \int_{-\infty}^{\infty} F(k_x, k_y) \exp(-ik_x x - ik_y y) dk_x dk_y \quad (1.39)$$

where the transform variables are spatial variables, x, y (in m), and spatial radian frequencies, k_x, k_y (in rad m^{-1}). We can now rewrite the *Fresnel diffraction formula* (see Eq. (1.35)) in terms of Fourier transform:

$$\begin{aligned} \psi_p(x, y; z) = & \exp(-ik_0 z) \frac{ik_0}{2\pi z} \exp\left[\frac{-ik_0}{2z}(x^2 + y^2)\right] \\ & \times \mathcal{F}\left\{\exp\left[\frac{-ik_0}{2z}(x^2 + y^2)\right] \psi_{p0}(x, y)\right\}_{k_x=\frac{k_0 x}{z}, k_y=\frac{k_0 y}{z}} \end{aligned} \quad (1.40)$$

Similarly, the Fraunhofer diffraction formula given by Eq. (1.37) can be written as

$$\psi_p(x, y; z) = \exp(-ik_0 z) \frac{ik_0}{2\pi z} \exp\left[\frac{-ik_0}{2z}(x^2 + y^2)\right] \mathcal{F}\{\psi_{p0}(x, y)\}_{k_x=\frac{k_0 x}{z}, k_y=\frac{k_0 y}{z}} \quad (1.41)$$

Figure 1.10 shows the simulation of Fresnel diffraction of a circular aperture function $\text{circ}(r/r_0)$, that is, $\psi_{p0}(x, y) = \text{circ}(r/r_0)$, where $r = \sqrt{x^2 + y^2}$ and $\text{circ}(r/r_0)$ denotes a value 1 within a circle of radius r_0 and 0 otherwise. The used wavelength for simulations is $0.6 \mu\text{m}$. Since $\psi_p(x, y; z)$ is a complex function, we plot its absolute value in the figures. Physically, the situation corresponds to the incidence of a plane wave with unit amplitude on an opaque screen with a circular opening of radius r_0 as $\psi_{p0}(x, y) = 1 \times t(x, y)$ with $t(x, y) = \text{circ}(r/r_0)$. We would then observe the intensity pattern, which is proportional to $|\psi_p(x, y; z)|^2$, at distance z away from the aperture. In Figure 1.11, we show Fraunhofer diffraction. We have chosen the distance of 80 cm so that the Fraunhofer approximation from Eq. (1.36) is satisfied.

1.6.1

Ideal Thin Lens as Optical Fourier Transformer

An ideal thin lens is a phase object, which means that it will only affect the phase of the incident light. For an ideal converging lens having a focal length f , the phase function of the lens is given by

$$t_f(x, y) = \exp\left[\frac{ik_0}{2f}(x^2 + y^2)\right] \quad (1.42)$$

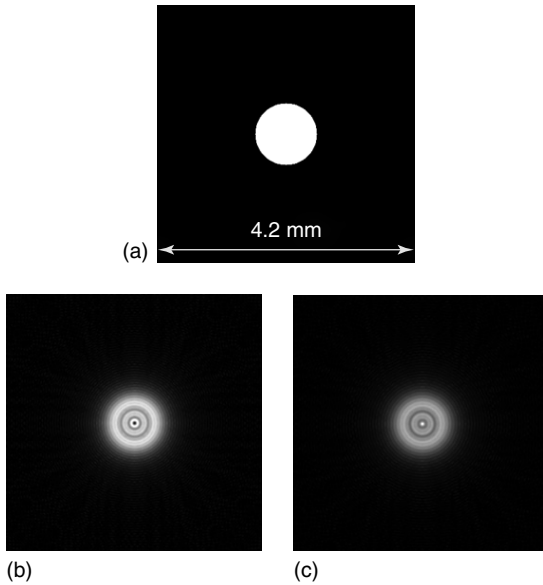


Figure 1.10 (a) Aperture function in the form of $\text{circ}(r/r_0)$, $r_0 = 1$ mm. (b) Diffraction at $z = 7$ cm (Fresnel diffraction), $|\psi_p(x, y; z = 7 \text{ cm})|$. (c) Diffraction at $z = 8$ cm (Fresnel diffraction), $|\psi_p(x, y; z = 8 \text{ cm})|$.

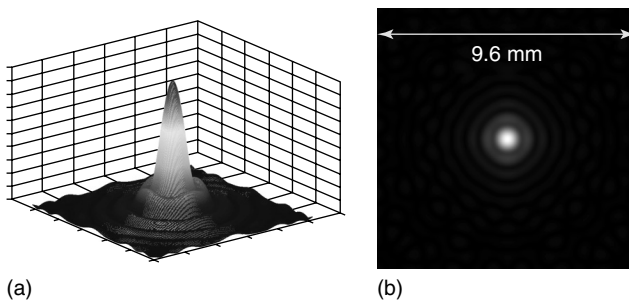


Figure 1.11 (a) 3D plot of a diffraction pattern at $z = 80$ cm (Fraunhofer diffraction), $|\psi_p(x, y; z = 80 \text{ cm})|$. (b) Gray-scale plot of $|\psi_p(x, y; z = 80 \text{ cm})|$. (Please find a color version of this figure on the color plates.)

where we have assumed that the lens is of infinite extent. For a uniform plane wave incident upon the lens, we can calculate the field distribution in the back focal plane of the lens using Eq. (1.34). To employ Eq. (1.34), we need to find the initial condition of the complex wave, which is given by $\psi_{p0}(x, y) = A \times t(x, y)$, the amplitude of the incident plane wave multiplied by the transparency function of the aperture. In the present case, $A = 1$ and the transparency function of the aperture is now given by the lens function $t_f(x, y)$, that is, $t(x, y) = t_f(x, y)$. Hence

$\psi_{p0}(x, y) = A \times t(x, y) = 1 \times t_f(x, y) = t_f(x, y)$. The field distribution at a distance f away from the lens, according to Eq. (1.34) with $z = f$ in $h(x, y, z)$, is then given by

$$\begin{aligned} \psi_p(x, y, f) &= t_f(x, y) * h(x, y, f) \\ &= \exp\left[\frac{ik_0}{2f}(x^2 + y^2)\right] * \exp(-ik_0f) \frac{ik_0}{2\pi f} \exp\left[\frac{-ik_0}{2f}(x^2 + y^2)\right] \end{aligned} \quad (1.43)$$

The above equation can be shown on evaluation to be proportional to a delta function, $\delta(x, y)$ [8], which is consistent with the geometrical optics that already states that all input rays parallel to the optical axis converge behind the lens to a point called the *back focal point*. The discussion thus far in a sense justifies the functional form of the phase function of the lens given by Eq. (1.42). We now look at a more complicated situation shown in Figure 1.12a, where a transparency $t(x, y)$ illuminated by a plane wave of unit amplitude is located in the front focal plane. We want to find the field distribution in the back focal plane. In Figure 1.12b, we describe the process of finding the field using a block diagram. Assuming that $t(x, y)$ is illuminated by a plane wave of unity, the field immediately after $t(x, y)$ is given by $1 \times t(x, y)$. The resulting field then undergoes Fresnel diffraction at a distance f , and according to Figure 1.9, $1 \times t(x, y)$ is the input to the block $h(x, y, f)$ as shown in Figure 1.12a. The diffracted field, $t(x, y) * h(x, y, f)$, is now immediately in front of the lens with a phase function given by $t_f(x, y)$, and hence the field after the lens is $[t(x, y) * h(x, y, f)] \times t_f(x, y)$. Finally, the field at the back focal plane is found using Fresnel diffraction one more time for a distance f , which is shown in Figure 1.12b. The resulting field is

$$\psi_p(x, y, f) = \{[t(x, y) * h(x, y, f)]t_f(x, y)\} * h(x, y, f) \quad (1.44)$$

The above equation can be worked out to become [8], apart from some constant,

$$\psi_p(x, y, f) = \mathcal{F}\{t(x, y)\}_{k_x=\frac{k_0x}{f}, k_y=\frac{k_0y}{f}} = T\left(\frac{k_0x}{f}, \frac{k_0y}{f}\right) \quad (1.45)$$

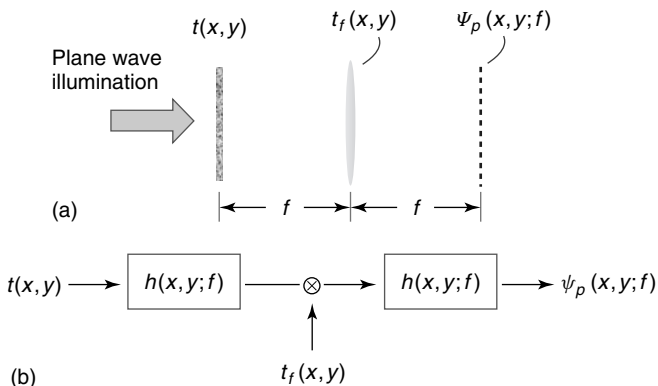


Figure 1.12 (a) Optical Fourier transformer: $\psi_p(x, y, f)$ is proportional to the Fourier transform of $t(x, y)$. (b) Block diagram for the physical system shown in (a).

where $T\left(\frac{k_0x}{f}, \frac{k_0y}{f}\right)$ is the Fourier transform or the *spectrum* of $t(x, y)$. We see that we have the exact Fourier transform of the “input,” $t(x, y)$, on the back focal plane of the lens. Hence an ideal thin lens is an optical Fourier transformer.

1.6.2

Imaging and Optical Image Processing

Figure 1.12a is the backbone of an optical image processing system. Figure 1.13 shows a standard image processing system with Figure 1.12a as the front end of the system. Figure 1.13 is the same optical system we have studied before in geometrical optics (Figure 1.6) except for the additional transparency function, $p(x, y)$, on the confocal plane. $p(x, y)$ is called the *pupil function* of the optical system. Now we analyze the system using the wave optics approach. On the input plane, we have an image in the form of a transparency, $t(x, y)$, which is assumed to be illuminated by a plane wave. Hence, according to Eq. (1.45), we have its spectrum on the back focal plane of lens L_1 , $T\left(\frac{k_0x}{f_1}, \frac{k_0y}{f_1}\right)$, where T is the Fourier transform of $t(x, y)$. Hence the confocal plane of the optical system is often called the *Fourier plane*. The spectrum of the input image is now modified by the pupil function, and the field immediately after the pupil function is $T\left(\frac{k_0x}{f_1}, \frac{k_0y}{f_1}\right)p(x, y)$. According Eq. (1.45) again, this field will be Fourier transformed to give the field on the image plane as

$$\psi_{\text{pi}} = \mathcal{F}\left\{T\left(\frac{k_0x}{f_1}, \frac{k_0y}{f_1}\right)p(x, y)\right\}_{k_x=\frac{k_0x}{f_2}, k_y=\frac{k_0y}{f_2}} \quad (1.46)$$

which can be evaluated, in terms of convolution, to give

$$\begin{aligned} \psi_{\text{pi}}(x, y) &= t\left(\frac{x}{M}, \frac{y}{M}\right) * \mathcal{F}\{p(x, y)\}_{k_x=\frac{k_0x}{f_2}, k_y=\frac{k_0y}{f_2}} \\ &= t\left(\frac{x}{M}, \frac{y}{M}\right) * P\left(\frac{k_0x}{f_2}, \frac{k_0y}{f_2}\right) \\ &= t\left(\frac{x}{M}, \frac{y}{M}\right) * h_C(x, y) \end{aligned} \quad (1.47)$$

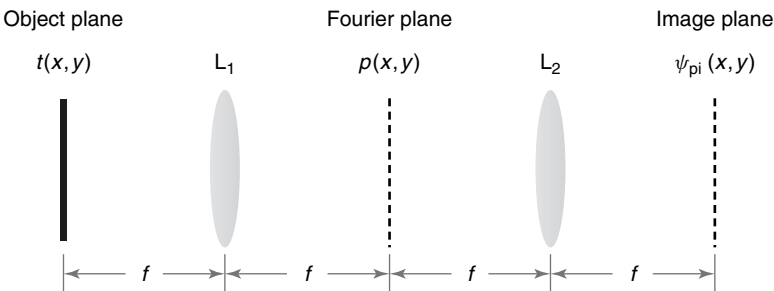


Figure 1.13 Optical image processing system.

where $M = -\frac{f_2}{f_1}$ as is the case for the two-lens imaging system in Figure 1.6 and P is the Fourier transform of p . From Eq. (1.47), we can recognize that

$$h_C(x, y) = \mathcal{F}\{p(x, y)\}_{k_x=\frac{k_0x}{f_2}, k_y=\frac{k_0y}{f_2}} = P\left(\frac{k_0x}{f_2}, \frac{k_0y}{f_2}\right) \quad (1.48)$$

is the point spread function in the context of a linear and spatial invariant system. In optics, it is called the *coherent point spread function*. Hence, the expression given by Eq. (1.47) can be interpreted as the result of a linear and spatial invariant system in that the scaled image of $t(x, y)$ is processed by an impulse response given by Eq. (1.48). The impulse response, and therefore the image processing capabilities, can be varied by simply changing the pupil function, $p(x, y)$. For example, if we take $p(x, y) = 1$, which means we do not modify the spectrum of the input image, then, $h_C(x, y)$, according to Eq. (1.48), becomes a delta function and the output image from Eq. (1.47) is $\psi_{\text{pi}}(x, y) \propto t\left(\frac{x}{M}, \frac{y}{M}\right) * \delta(x, y) = t\left(\frac{x}{M}, \frac{y}{M}\right)$. The result is an image scaled by M , consistent with the result obtained from geometrical optics.

If we now take $p(x, y) = \text{circ}(r/r_0)$, then, from the interpretation of Eq. (1.46), we see that for this kind of chosen pupil, filtering is of low-pass characteristic as the opening of the circle on the pupil plane only allows physically the low spatial frequencies to go through. Figure 1.14 shows examples of low-pass filtering. In Figure 1.14a,b, we show the original of the image and its spectrum, respectively. In Figure 1.14c,e, we show the filtered images, and their low-pass filtered spectra are shown in Figure 1.14d,f, respectively, where the low-pass filtered spectra are obtained by multiplying the original spectrum by $\text{circ}(r/r_0)$. Note that the radius r_0 in Figure 1.14d is larger than that in Figure 1.14f. In Figure 1.15, we show high-pass filtering examples where we take $p(x, y) = 1 - \text{circ}(r/r_0)$.

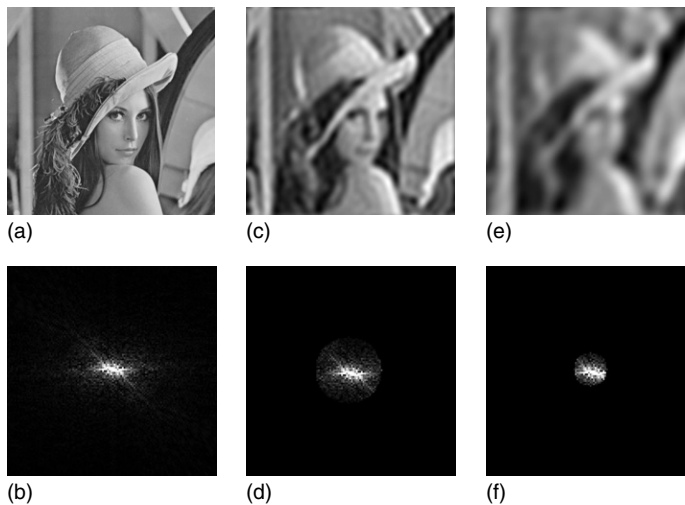


Figure 1.14 Low-pass filtering examples: (a) original image, (b) spectrum of (a), (c) and (e) low-pass images, (d) and (f) spectrum of (c) and (e), respectively.

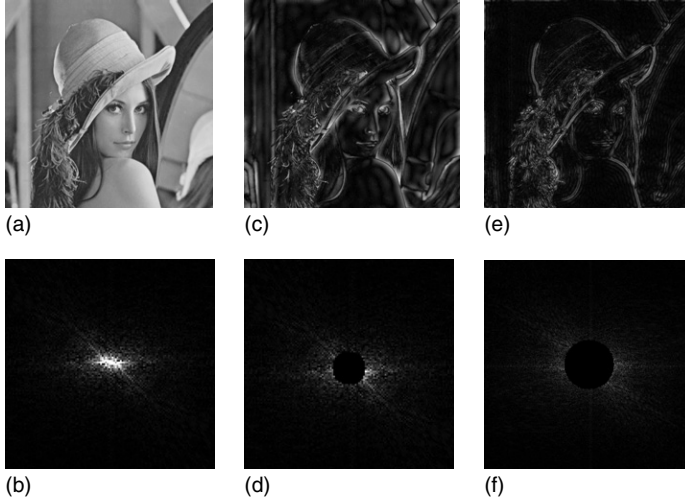


Figure 1.15 Same as in Figure 1.14, but with high-pass filtering.

1.6.3

Optical Correlator

The correlation of two images is one of the most important mathematical operations in pattern recognition [9]. However, as the images become more and more complex and large in size, the calculation becomes time consuming for a digital computer. Optical processing provides an alternative to digital processing as it offers greater speed. For images $g_1(x, y)$ and $g_2(x, y)$, the correlation between them is given by

$$g_1(x, y) \otimes g_2(x, y) = \int_{-\infty}^{\infty} \int_{-\infty}^{\infty} g_1^*(x', y') g_2(x + x', y + y') dx' dy' \quad (1.49)$$

where $g_1^*(x, y)$ is the complex conjugate of $g_1(x, y)$ and \otimes denotes the operation of correlation. The role of *optical correlators* is to implement Eq. (1.49) optically. In this section, we describe an optical correlator called the *joint-transform correlator*. Figure 1.16 shows a standard optical correlator. $g_1(x, y)$ and $g_2(x, y)$ are the two images to be correlated, and they are in the form of transparencies, which are illuminated by plane waves. They are separated by a distance of $2x_0$ in the front focal plane of Fourier transform lens L_1 as shown in Figure 1.16. The so-called joint-transform power spectrum, JTPS(k_x, k_y), on the back focal plane of lens L_1 is given by

$$\text{JTPS}(k_x, k_y) = |\mathcal{F}\{g_1(x + x_0, y)\} + \mathcal{F}\{g_2(x - x_0, y)\}|^2 \quad (1.50)$$

The expression in Eq. (1.50) is essentially the intensity pattern on the focal plane. Expanding Eq. (1.50), we have

$$\begin{aligned} \text{JTPS}(k_x, k_y) = & |\hat{g}_1(k_x, k_y)|^2 + |\hat{g}_2(k_x, k_y)|^2 + \hat{g}_1^*(k_x, k_y) \hat{g}_2(k_x, k_y) \exp(i2k_0 x_0) \\ & + \hat{g}_1(k_x, k_y) \hat{g}_2^*(k_x, k_y) \exp(-i2k_0 x_0) \end{aligned} \quad (1.51)$$

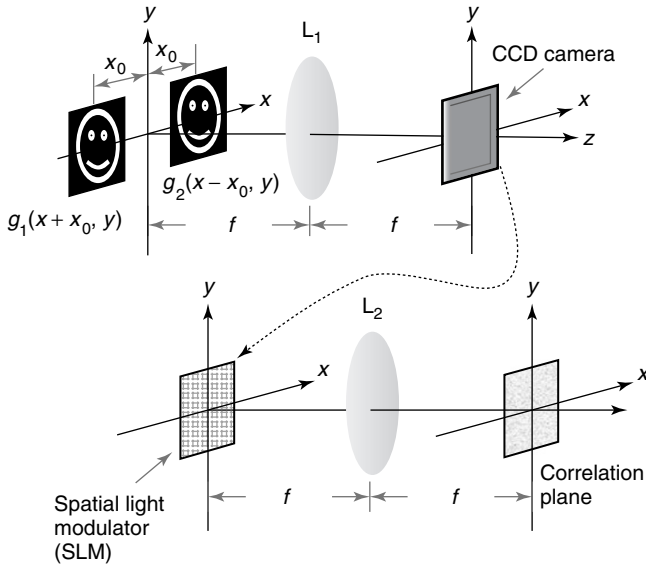


Figure 1.16 Optical correlator.

where $\hat{g}_1(k_x, k_y)$ and $\hat{g}_2(k_x, k_y)$ are the Fourier transform of g_1 and g_2 , respectively with $k_x = k_0 x/f$ and $k_y = k_0 y/f$, where k_0 is the wavenumber of the plane wave. The joint-transform power spectrum (JTPS) is now detected by a CCD camera, whose output is fed to a 2D *spatial light modulator*. A 2D spatial light modulator is a device with which one can imprint a 2D pattern on a laser beam by passing the laser beam through it (or by reflecting the laser beam off it) [10]. A liquid crystal TV (LCTV) (upon suitable modification) is a good example of a spatial light modulator. In fact, we can think of a spatial light modulator as a real-time transparency because one can update 2D images on the spatial light modulator in real time without developing films into transparencies. The readers may refer to Chapter 9 of this book for more details of spatial light modulators. Once the JTPS is loaded to the spatial light modulator; we can then put the spatial light modulator in the front focal plane of Fourier transform lens L_2 as shown in Figure 1.16. The back focal plane of lens L_2 is the correlation plane as it shows all the correlation outputs. To see that, we take the Fourier transform of JTPS.

$$\begin{aligned} \mathcal{F} \left\{ \text{JTPS} \left(\frac{k_0 x}{f}, \frac{k_0 y}{f} \right) \right\}_{k_x = \frac{k_0 x}{f}, k_y = \frac{k_0 y}{f}} &= C_{11}(-x, -y) + C_{22}(-x, -y) \\ &+ C_{12}(-x - 2x_0, -y) + C_{21}(-x + 2x_0, -y) \end{aligned} \quad (1.52)$$

where

$$C_{mn}(x, y) = g_m \otimes g_n \quad (1.53)$$

with $m = 1$ or 2 , and $n = 1$ or 2 . $C_{mn}(x, y)$ is the autocorrelation when $m = n$, and is the cross-correlation when $m \neq n$. Therefore, if the two images g_m and g_n

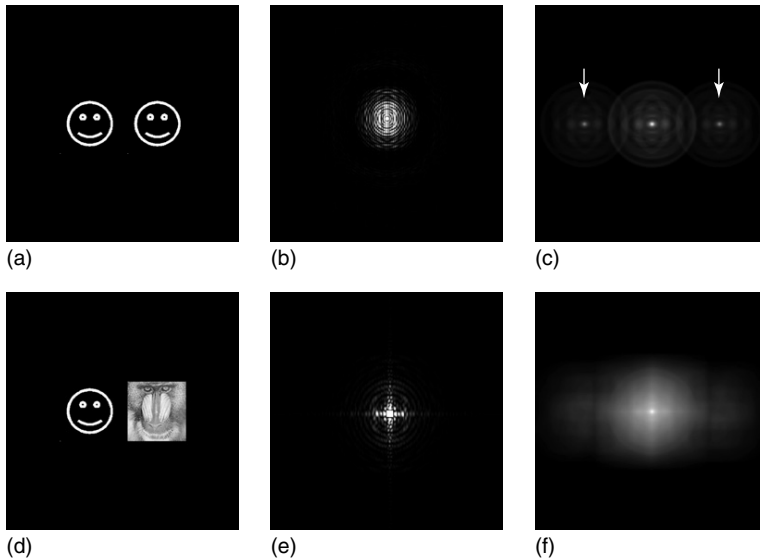


Figure 1.17 Simulation results for optical correlator shown in Figure 1.16. (a) Input patterns, (b) JTPS of the two input patterns, (c) output on the correlation plane, (d–f) are the same as in (a–c) but with the input patterns not identical.

are the same, besides a strong peak at the origin of the correlation plane due to the first two terms in Eq. (1.52), we have two strong peaks centered at $x = \pm 2x_0$. Figure 1.17a–c shows the input patterns, the JTPS (on the CCD camera plane), and the output on the correlation plane, respectively. Note that since the two input patterns are identical, we have two bright correlation spots (denoted by white arrows in the Figure 1.17c) on both sides of the center spot. Figure 1.17d–f is similar to Figure 1.17a–c, respectively but the two input patterns are different. Note that there are no discernible bright spots on both sides of the output in the center of the correlation plane in the case of mismatched patterns in the input plane.

1.7

The Human Visual System

Figure 1.18 is a schematic diagram of a human eye. The cornea and the crystalline lens together serve as a converging lens in the imaging system. To control the entering light flux, there is an iris between the cornea and the lens. The diameter of the iris can vary from about 2 to 8 mm. The crystalline lens is connected with several ciliary muscles in order to alter the shape of the crystalline lens so that the effective focal length of the lens can be adjusted. The eye is relaxed when it is focused on an infinitely distant object. When a person looks at an object, his brain will automatically control the ciliary muscles to focus the image on the

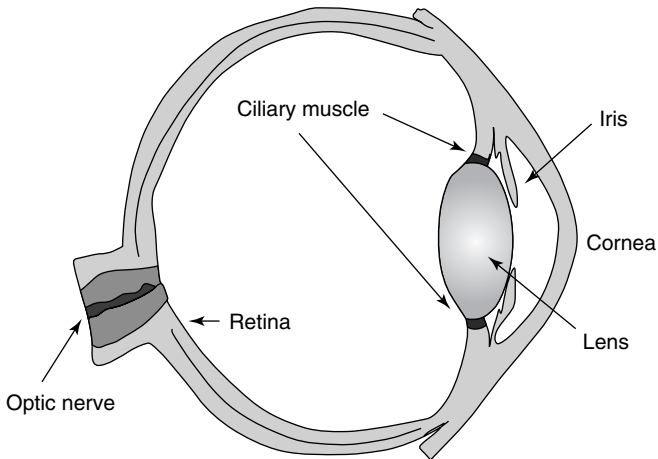


Figure 1.18 Cross section of the human eye.

retina clearly. The retina is a film that consists of numerous light-sensitive cells. Its function is to transform the illuminating light to an electric signal – like the CCD sensor in a digital camera. The electric signal is delivered to the brain via the optic nerve, and is finally read and analyzed by the brain.

The human eye can measure not only light strength but also colors because the retina contains two classes of receptors, the rods and the cones. Rods are very sensitive to weak light, but cannot identify colors. In contrast to the rods, the cones are insensitive to the weak light but can identify colors. This is because there are three different types of cones, and they are respectively sensitive to red light, green light, and blue light. The sensitivity spectrum of a normal human eye is roughly between 390 and 780 nm. Owing to the various responses of the receptors, it is interesting that the most sensitive wavelength of human eye is 555 nm in daytime, but is 507 nm at night. Some people's retina is short of one or more types of cones, and thus they cannot identify colors correctly. This is called "*color blindness*." Although most people own complete cones and rods, their color experiences are usually different from one another. This is one of the major challenges in color engineering [11, 12].

There are several kinds of abnormal eyes: nearsightedness, farsightedness, and astigmatism. Nearsightedness and farsightedness are both due to the defocus aberration of the eye. In the former case, the image of an object that is far away is formed in front of the retina, and in the latter case the image is formed in the back of the retina. Astigmatism of the eye is different from astigmatism aberration that we mentioned in Section 1.3.3. For an eye with astigmatism, its cornea is asymmetric. Thus for a distant point object, the image formed on the retina will be an asymmetric and elliptical spot.

The above-mentioned abnormal eyes result in blurred images, which can be corrected by glasses [2]. Note that the iris serves as an aperture stop of the lens so that aberrations can be adjusted. People with nearsightedness or farsightedness

see clearer in daytime (smaller iris) than at night (larger iris). They are also used to squinting for clearer vision.

1.8

Conclusion

This chapter has provided some of the fundamentals and applications in optical image processing. When diffraction is of no concern in the imaging systems, we can use geometrical optics to explain the imaging process using matrix formalism. However, the matrix formalism is only applicable for paraxial rays. To consider the effect of diffraction, we need to use wave optics. Wave optics can be formulated in terms of the Fresnel diffraction formula, which can be reformulated using Fourier transforms. Hence image formation and image processing can be described in terms of Fourier transforms, which is the basis of what is known as *Fourier optics*. However, the use of Fourier optics is only applicable under the paraxial approximation. Nevertheless, Fourier optics is widely used and one of its most important applications is in the area of optical correlation. We have discussed an optical correlation architecture called *joint-transform correlator*, which has provided an important example on how one can use Fourier optics in the treatment of optical image processing.

References

1. Hudson, R.D. (1969) *Infrared System Engineering*, John Wiley & Sons, Inc., New York.
2. Hecht, E. (2002) *Optics*, Addison-Wesley, San Francisco.
3. Hecht, J. (2008) The history of the X-ray laser. *Opt. Photonics News*, **19** (4), 26–33.
4. Poon, T.-C. and Kim, T. (2006) *Engineering Optics with MATLAB*, World Scientific, Singapore.
5. Smith, W.J. (2008) *Modern Optical Engineering*, SPIE Press, New York.
6. Mahajan, V.N. (1998) *Optical Imaging and Aberrations*, SPIE Press, Bellingham.
7. Born, M. and Wolf, E. (1999) *Principles of Optics*, Cambridge University Press, Cambridge.
8. Poon, T.-C. (2007) *Optical Scanning Holography with MATLAB*, Springer, New York.
9. Yu, F.T.S. and Jutamulia, S. (1998) *Optical Pattern Recognition*, Cambridge University Press, Cambridge.
10. Poon, T.-C. *et al.* (1998) Spatial light modulators-research, development, and applications: introduction to the feature issue. *Appl. Opt.*, **37**, 7471.
11. Wyszecki, G. and Stiles, W.S. (1982) *Color Science*, John Wiley & Sons, Inc., New York.
12. Shevell, S.K. (2003) *The Science of Color*, Elsevier, Amsterdam.

